Supplement of Atmos. Meas. Tech., 10, 1203–1213, 2017
http://www.atmos-meas-tech.net/10/1203/2017/
doi:10.5194/amt-10-1203-2017-supplement

Atmospheric Measurement Techniques
Open Access
EGU

Supplement of

Calibration of a multi-pass photoacoustic spectrometer cell using light-absorbing aerosols

Nir Bluvshtein et al.

Correspondence to: Yinon Rudich (yinon.rudich@weizmann.ac.il)

Validation of 404 nm multi-pass photoacoustic spectrometer

We tested the linearity of the PAS response for slightly absorbing particles. Figure S1 shows the change in signal (relative to the baseline of N_2 filled cell) for 200 nm particles of Suwannee River fulvic acid (SRFA), and 150 nm and 250 nm particles of Pahokee Peat fulvic acid at different concentrations. At the tested concentration range linearity is maintained. The PAS response to purely scattering substances at the relevant wavelength was also measured. We tested the PAS response to PSL spheres and ammonium sulfate particles and found no increase in the measured signal when these particles were introduced.

Figure S2 shows that the baseline and PAS response for four PSL sizes cannot be distinguished. We also found that the PAS measurement is stable at low RH (0-12%), for flow rates of 300-1500 cm^3 min^{-1} and that slightly absorbing particles (SRFA and PPFA in this case) are not modified by the interaction with the high laser power. The latter was verified by testing the stability of the particles extinction in the CRD-S as they were alternately subjected to the high intensity PAS laser beam.

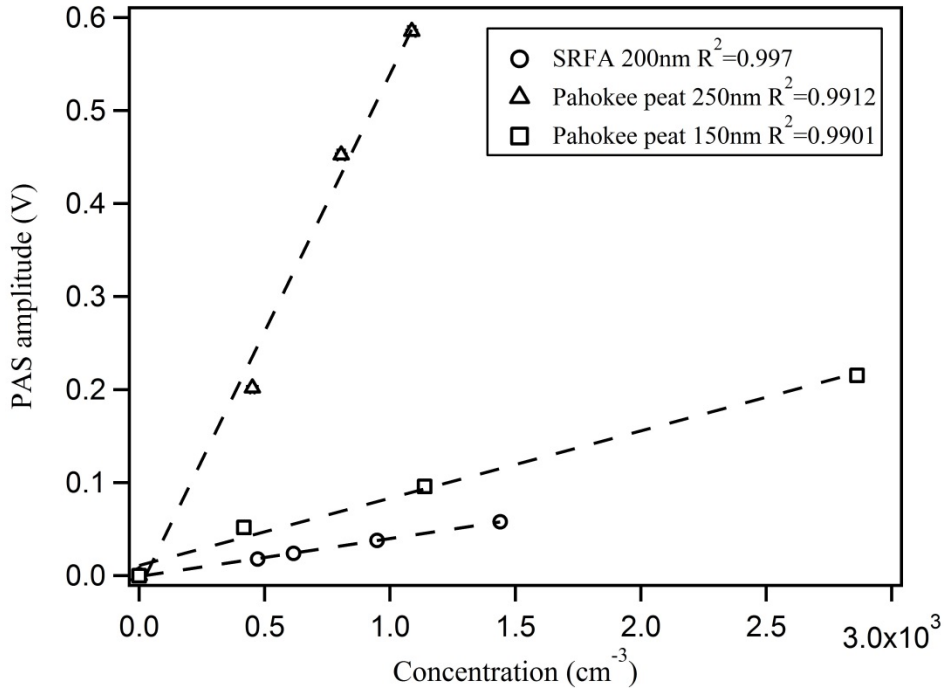

Figure S1: PAS cell linear response. The PAS signal (amplitude) was measured as a function of particle concentration.

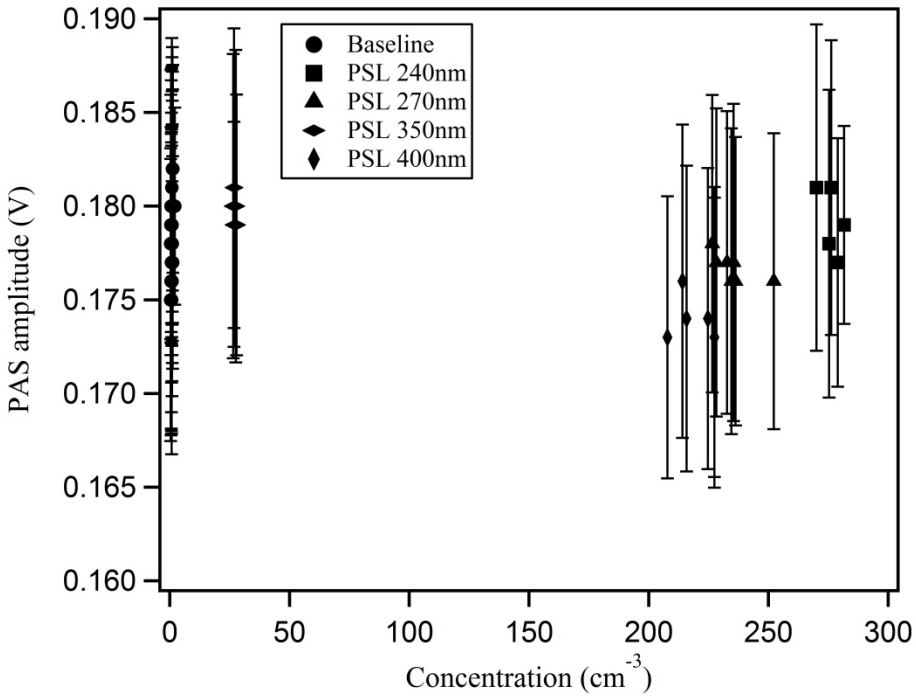

Figure S2: PAS cell baseline and response to purely scattering particles at different diameters and concentrations. Error bars represent calculated standard error for 120 sec measurements.

Validation of the 404 nm cavity ring down spectrometer

To validate the new 404 nm CRD-S, the light intensity decay in the cavity is monitored and an exponential function is fitted to the signal (Figure S3). As a rule of thumb, the fit should yield $R^2 \geq 0.9999$ and a residual $\leq 10\%$ in a time span of at least five times the calculated decay time (τ). Additionally, the linearity of the calculated extinction was tested by plotting the extinction coefficient as a function of particle concentration when a single component quasi-monodispersed particle population was introduced to the cavity (Figure S4). The proportionality constant of such a plot is the extinction cross section (σ_{ext}) of the particle. In Figure S4, σ_{ext}'s (slopes of the shown curves) are not shown because the particles used are not PSL spheres so σ_{ext} may suffer from multiply charged particles contribution. If corrected, it is expected to improve linearity.

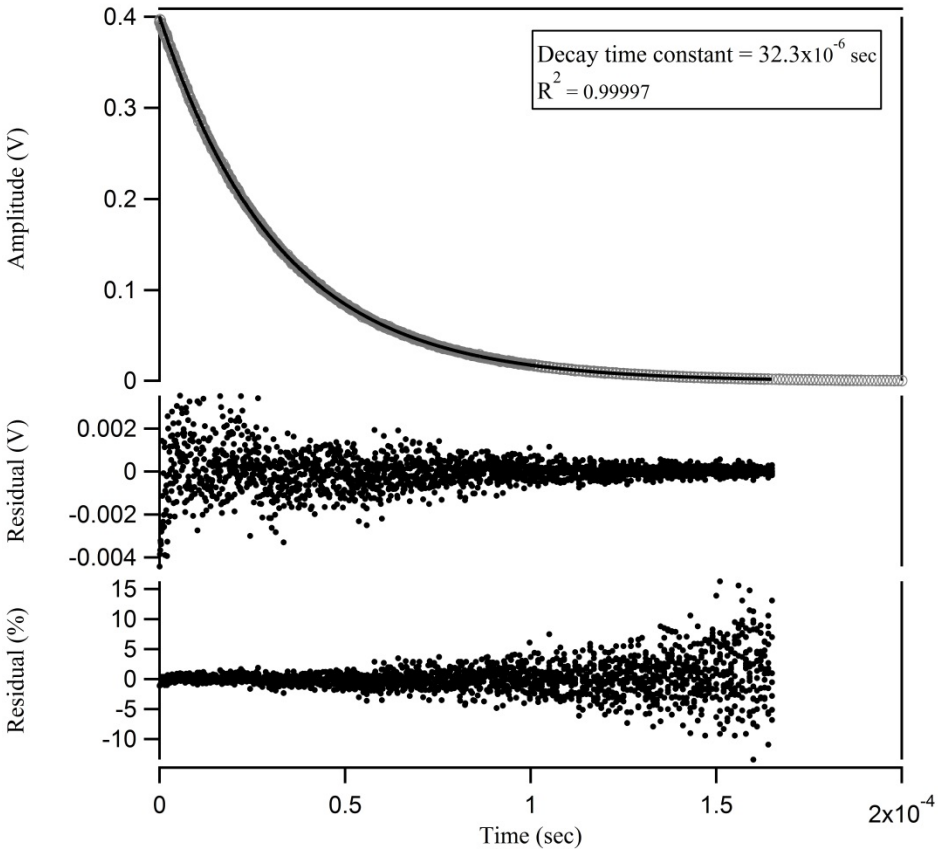

Figure S3: Validation of the 404 nm wavelength CRD-S. Measured intensity decay in a nitrogen filled cavity (gray circles) fitted to an exponential decay (black solid line) with time constant $\tau_0 = 32.3\times10^{-6}$ sec and $R^2 > 0.9999$ up to about 1.6×10^{-4} sec. The residual is mostly below 10% of the measured intensity.

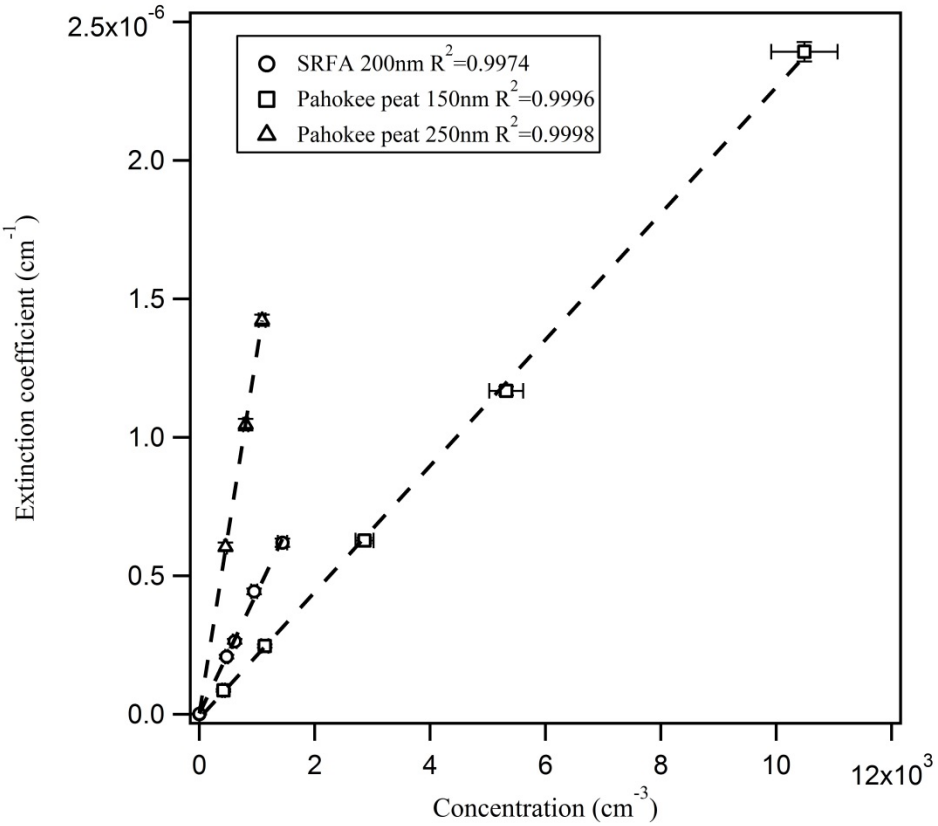

Figure S4: CRD-S linear response. The extinction coefficient (α_{ext}) was measured as a function of particle concentration. The extinction cross section (σ_{ext}) can be extracted from the slope of the linear fit (following extinction correction duo to multiply charged particles).

Ozone production and PAS calibration

To test O_3 loss in each of the PA-CRD-S components, 627 ppm of O_3 was generated using the UV lamp O_3 generator with 0.1 LPM of high purity (99.999%) O_2 gas as described in the main text and measured with an O_3 monitor (model 106-L, 2B technologies, CO, U.S.A) following a 10 fold dilution with dry N_2. Results showed ≈1.6% loss in the PAS cell with the laser turned off and ≈3% with the laser turned on at its highest power output. Results also showed that no measureable loss could be detected due to flow in the CRD-S with the laser turned on and off.

Additionally, the absorption coefficient from the CRD-S was recorded as the laser light was blocked and un-blocked from entering the PAS cell with O_3 flow from the UV lamp generator in the "PAS first" tandem configuration. Figure S6 shows that the measured absorption coefficient in the CRD-S increased by 0.5 to 1% when laser power was blocked from the PAS cell suggesting some ozone photolysis.

A comparison between O_3 calibrations at different instrumental configurations is shown in Figure S5. O_3 calibration curves are shown for a "PAS first" and a "CRD-S first" tandem setups where O_3 was generated using both the UV lamp and the corona discharge generators. Differences between the calibration slopes are below 5%.

To test whether the O_3 concentration is stable with laser power, we used O_2/O_3 flow from the UV lamp with about 627 ppm O_3 and varied the set laser power. Figure S7 demonstrates the linearity of the PAS cell response with variation in laser power and rules out non-linear processes related to laser power which may cause errors in PA-CRD-S O_3 calibration. In this figure, we show the PAS signal (not normalized by laser intensity) as a function of the laser intensity measured by the photodiode at the back mirror of the PAS cell.

Additionally, to validate the stability of the O_3 calibration procedure at different flow rates we have performed O_3 calibration using the corona discharge generator in a tandem "PAS first" configuration at flow rates of 100, 300, 600, 900 cc min^{-1}. Resultant calibration slopes were 3.967×10^{-7}, 4.047×10^{-7}, 3.985×10^{-7}, 4.020×10^{-7} cm^{-1} V^{-1} respectively, confirming that in our system O_3 calibration slope is independent of the flow rate within our experimental conditions.

The different calibration tests described above were performed with significant time interval of weeks to months between them. Occasionally the PAS cell is disassembled, cleaned and realigned. Changes in cleanliness of the windows, mirrors, microphone and difference in wall scattering due to different alignment may cause changes to the instrument response and consequently to the calculated calibration curve. This is demonstrated in our study by the difference in O_3 calibration slope between figure 5, figure S5 and the results of the calibration slopes with changing flow rates.

From the above results, we conclude that the effect of possible NO_2 (or other gas) contamination due to O_3 generation, if exists, is negligible.

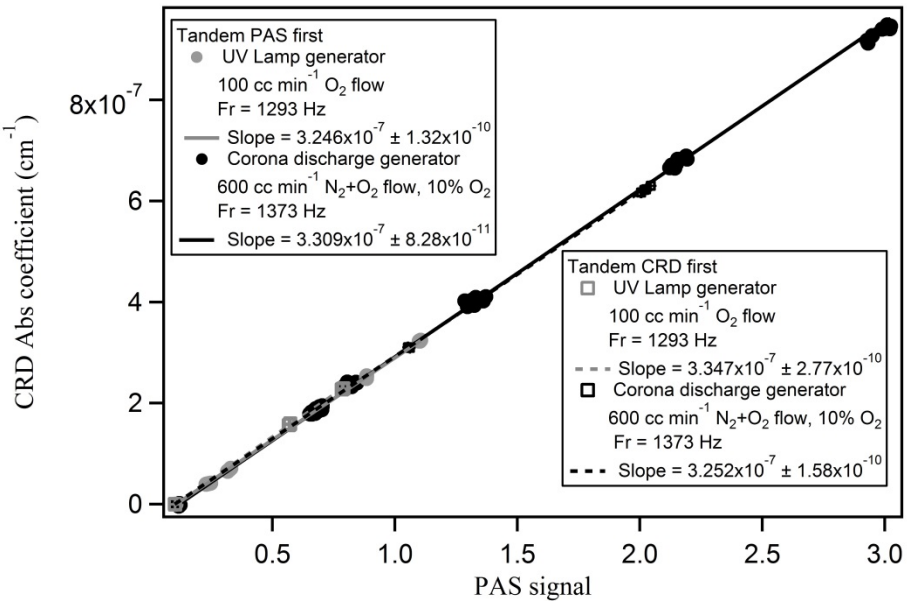

Figure S5: O_3 calibration curves of the PAS-CRD-S system at different instrumental configuration.

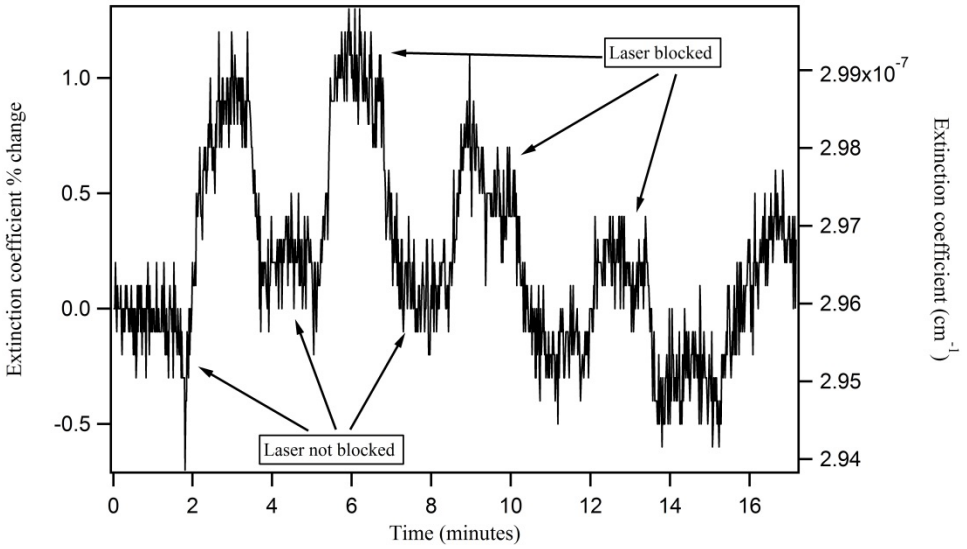

Figure S6: Change in CRD-S extinction coefficient in response to blocking the laser light from entering the PAS.

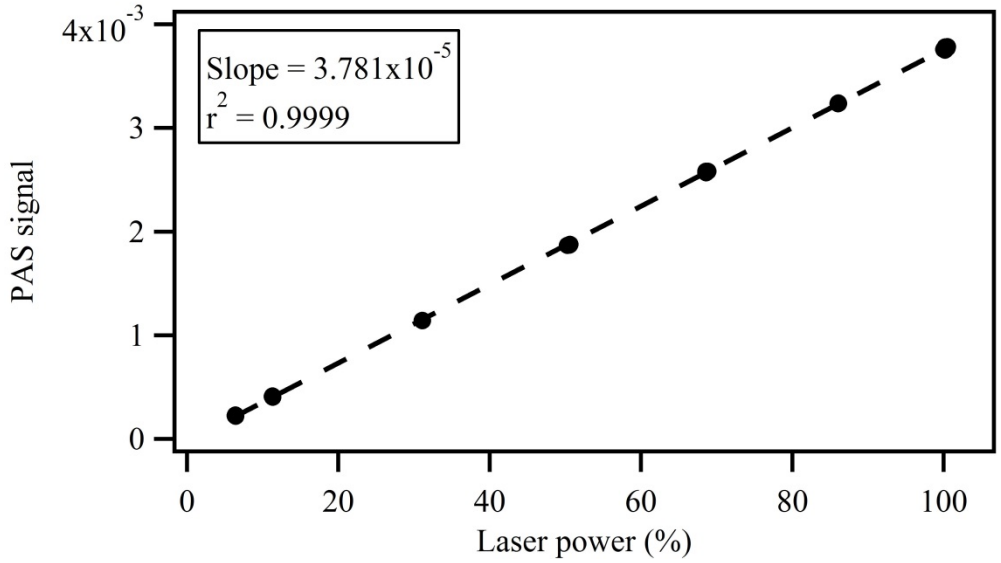

Figure S7: PAS signal (not normalized to the measured laser power) changing in response to changing the laser power set point with the Toptica user interface software (TopControl). The relative laser power on the x axis is inferred from the measured and not the set point laser power.

Complex refractive index retrieval for nigrosin thin film using Spectroscopic ellipsometer measurements

Table S1: Retrieved complex RI retrieved from SE measurement of the single sample presented in Figure 4 in the main text.

Wavelength (nm)	Real part	Imaginary part
301	1.644 ± 0.0097	0.2865 ± 0.0123
302	1.65 ± 0.0097	0.286 ± 0.0123
304	1.655 ± 0.0089	0.2849 ± 0.0122
306	1.661 ± 0.0086	0.2834 ± 0.012
307	1.667 ± 0.0082	0.2814 ± 0.0119
309	1.672 ± 0.0079	0.2789 ± 0.0117
310	1.678 ± 0.0077	0.2759 ± 0.0115
312	1.682 ± 0.0075	0.2726 ± 0.0113
314	1.687 ± 0.0073	0.269 ± 0.011
315	1.691 ± 0.0071	0.265 ± 0.0108
317	1.695 ± 0.007	0.2608 ± 0.0106
318	1.699 ± 0.0069	0.2563 ± 0.0103
320	1.702 ± 0.0069	0.2516 ± 0.0101
322	1.705 ± 0.0068	0.2468 ± 0.0099
323	1.707 ± 0.0068	0.2418 ± 0.0097
325	1.709 ± 0.0069	0.2368 ± 0.0096

326	1.711 ± 0.0069	0.2317 ± 0.0094
328	1.712 ± 0.007	0.2266 ± 0.0093
330	1.713 ± 0.007	0.2216 ± 0.0091
331	1.714 ± 0.0071	0.2165 ± 0.009
333	1.714 ± 0.0072	0.2115 ± 0.0089
334	1.714 ± 0.0073	0.2067 ± 0.0088
336	1.714 ± 0.0075	0.2019 ± 0.0088
338	1.713 ± 0.0076	0.1973 ± 0.0087
339	1.712 ± 0.0077	0.1928 ± 0.0087
341	1.711 ± 0.0078	0.1885 ± 0.0086
342	1.71 ± 0.0079	0.1843 ± 0.0086
344	1.708 ± 0.0081	0.1804 ± 0.0086
346	1.706 ± 0.0082	0.1766 ± 0.0086
347	1.704 ± 0.0083	0.1731 ± 0.0086
349	1.702 ± 0.0083	0.1697 ± 0.0086
350	1.7 ± 0.0084	0.1666 ± 0.0086
352	1.697 ± 0.0085	0.1636 ± 0.0086
354	1.695 ± 0.0085	0.1609 ± 0.0086
355	1.692 ± 0.0086	0.1584 ± 0.0086
357	1.69 ± 0.0086	0.1561 ± 0.0086
358	1.687 ± 0.0086	0.154 ± 0.0086
360	1.684 ± 0.0086	0.1521 ± 0.0086
362	1.682 ± 0.0086	0.1504 ± 0.0086
363	1.679 ± 0.0086	0.1489 ± 0.0087
365	1.676 ± 0.0085	0.1476 ± 0.0087
366	1.673 ± 0.0085	0.1464 ± 0.0087
368	1.671 ± 0.0084	0.1455 ± 0.0087
370	1.668 ± 0.0083	0.1446 ± 0.0087
371	1.665 ± 0.0083	0.144 ± 0.0088
373	1.663 ± 0.0082	0.1435 ± 0.0088
374	1.66 ± 0.0081	0.1431 ± 0.0088
376	1.657 ± 0.008	0.1429 ± 0.0088
378	1.655 ± 0.0079	0.1428 ± 0.0089
379	1.653 ± 0.0077	0.1428 ± 0.0089
381	1.65 ± 0.0076	0.143 ± 0.0089
382	1.648 ± 0.0075	0.1432 ± 0.0089
384	1.646 ± 0.0074	0.1436 ± 0.0089
386	1.644 ± 0.0073	0.144 ± 0.0088
387	1.642 ± 0.0072	0.1445 ± 0.0088
389	1.64 ± 0.0071	0.1451 ± 0.0088
390	1.638 ± 0.007	0.1458 ± 0.0087

392	1.636 ± 0.0069	0.1465 ± 0.0087
394	1.634 ± 0.0068	0.1473 ± 0.0086
395	1.632 ± 0.0067	0.1481 ± 0.0086
397	1.631 ± 0.0066	0.149 ± 0.0085
398	1.629 ± 0.0065	0.15 ± 0.0084
400	1.628 ± 0.0065	0.1509 ± 0.0083
402	1.626 ± 0.0064	0.152 ± 0.0083
403	1.625 ± 0.0064	0.153 ± 0.0082
405	1.624 ± 0.0063	0.1541 ± 0.0081
406	1.622 ± 0.0063	0.1552 ± 0.008
408	1.621 ± 0.0063	0.1563 ± 0.0079
410	1.62 ± 0.0063	0.1575 ± 0.0078
411	1.619 ± 0.0063	0.1586 ± 0.0076
413	1.618 ± 0.0063	0.1598 ± 0.0075
414	1.617 ± 0.0063	0.161 ± 0.0074
416	1.616 ± 0.0063	0.1622 ± 0.0073
418	1.615 ± 0.0064	0.1634 ± 0.0072
419	1.615 ± 0.0064	0.1646 ± 0.0071
421	1.614 ± 0.0064	0.1658 ± 0.007
422	1.613 ± 0.0065	0.1671 ± 0.0069
424	1.612 ± 0.0066	0.1683 ± 0.0068
426	1.612 ± 0.0066	0.1696 ± 0.0068
427	1.611 ± 0.0067	0.1708 ± 0.0067
429	1.61 ± 0.0068	0.1721 ± 0.0066
430	1.61 ± 0.0069	0.1733 ± 0.0065
432	1.609 ± 0.0069	0.1746 ± 0.0065
433	1.609 ± 0.007	0.1759 ± 0.0064
435	1.608 ± 0.0071	0.1772 ± 0.0064
437	1.608 ± 0.0072	0.1785 ± 0.0063
438	1.608 ± 0.0073	0.1798 ± 0.0063
440	1.607 ± 0.0074	0.1811 ± 0.0063
441	1.607 ± 0.0075	0.1824 ± 0.0062
443	1.606 ± 0.0076	0.1837 ± 0.0062
445	1.606 ± 0.0078	0.185 ± 0.0062
446	1.606 ± 0.0079	0.1864 ± 0.0062
448	1.605 ± 0.008	0.1877 ± 0.0062
449	1.605 ± 0.0081	0.1891 ± 0.0062
451	1.605 ± 0.0082	0.1905 ± 0.0063
453	1.605 ± 0.0083	0.1919 ± 0.0063
454	1.604 ± 0.0084	0.1933 ± 0.0063
456	1.604 ± 0.0085	0.1948 ± 0.0064

457	1.604 ± 0.0086	0.1962 ± 0.0064
459	1.604 ± 0.0087	0.1977 ± 0.0065
461	1.604 ± 0.0088	0.1992 ± 0.0065
462	1.604 ± 0.0089	0.2007 ± 0.0066
464	1.604 ± 0.009	0.2022 ± 0.0067
465	1.604 ± 0.0093	0.2037 ± 0.0067
467	1.604 ± 0.0094	0.2053 ± 0.0068
469	1.604 ± 0.0095	0.2069 ± 0.0069
470	1.604 ± 0.0096	0.2085 ± 0.007
472	1.604 ± 0.0097	0.2101 ± 0.0072
473	1.604 ± 0.0097	0.2118 ± 0.0073
475	1.604 ± 0.0098	0.2135 ± 0.0074
477	1.604 ± 0.0098	0.2152 ± 0.0076
478	1.604 ± 0.0099	0.2169 ± 0.0077
480	1.605 ± 0.0099	0.2186 ± 0.0079
481	1.605 ± 0.0099	0.2204 ± 0.008
483	1.605 ± 0.0099	0.2221 ± 0.0082
485	1.606 ± 0.0099	0.2239 ± 0.0083
486	1.606 ± 0.0099	0.2257 ± 0.0085
488	1.606 ± 0.0099	0.2276 ± 0.0087
489	1.607 ± 0.0099	0.2294 ± 0.0088
491	1.608 ± 0.0099	0.2313 ± 0.009
493	1.608 ± 0.0098	0.2331 ± 0.0092
494	1.609 ± 0.0098	0.235 ± 0.0093
496	1.61 ± 0.0097	0.2369 ± 0.0095
497	1.61 ± 0.0097	0.2388 ± 0.0096
499	1.611 ± 0.0096	0.2406 ± 0.0098
501	1.612 ± 0.0095	0.2425 ± 0.0099
502	1.613 ± 0.0094	0.2444 ± 0.0101
504	1.614 ± 0.0093	0.2463 ± 0.0102
505	1.615 ± 0.0092	0.2482 ± 0.0103
507	1.616 ± 0.0091	0.2501 ± 0.0105
509	1.617 ± 0.009	0.252 ± 0.0106
510	1.618 ± 0.0089	0.2539 ± 0.0107
512	1.62 ± 0.0087	0.2557 ± 0.0108
513	1.621 ± 0.0086	0.2576 ± 0.0109
515	1.622 ± 0.0085	0.2594 ± 0.011
517	1.624 ± 0.0083	0.2612 ± 0.0111
518	1.625 ± 0.0082	0.263 ± 0.0111
520	1.627 ± 0.008	0.2648 ± 0.0112
521	1.628 ± 0.0079	0.2665 ± 0.0112

523	1.63 ± 0.0077	0.2683 ± 0.0113
525	1.632 ± 0.0076	0.2699 ± 0.0113
526	1.634 ± 0.0074	0.2716 ± 0.0113
528	1.635 ± 0.0072	0.2732 ± 0.0113
529	1.637 ± 0.0071	0.2748 ± 0.0114
531	1.639 ± 0.0069	0.2764 ± 0.0114
533	1.641 ± 0.0068	0.2779 ± 0.0113
534	1.643 ± 0.0066	0.2794 ± 0.0113
536	1.645 ± 0.0064	0.2808 ± 0.0113
537	1.647 ± 0.0063	0.2822 ± 0.0112
539	1.65 ± 0.0061	0.2835 ± 0.0112
541	1.652 ± 0.006	0.2848 ± 0.0111
542	1.654 ± 0.0058	0.2861 ± 0.0111
544	1.656 ± 0.0057	0.2873 ± 0.011
545	1.659 ± 0.0055	0.2884 ± 0.0109
547	1.661 ± 0.0054	0.2895 ± 0.0109
548	1.663 ± 0.0052	0.2906 ± 0.0108
550	1.666 ± 0.0051	0.2915 ± 0.0107
552	1.668 ± 0.005	0.2925 ± 0.0106
553	1.671 ± 0.0048	0.2933 ± 0.0105
555	1.673 ± 0.0047	0.2942 ± 0.0103
556	1.675 ± 0.0046	0.2949 ± 0.0102
558	1.678 ± 0.0045	0.2956 ± 0.0101
560	1.681 ± 0.0043	0.2963 ± 0.01
561	1.683 ± 0.0042	0.2969 ± 0.0098
563	1.686 ± 0.0041	0.2974 ± 0.0097
564	1.688 ± 0.004	0.2979 ± 0.0096
566	1.691 ± 0.0039	0.2983 ± 0.0094
568	1.693 ± 0.0039	0.2986 ± 0.0093
569	1.696 ± 0.0038	0.2989 ± 0.0091
571	1.699 ± 0.0037	0.2992 ± 0.009
572	1.701 ± 0.0036	0.2994 ± 0.0089
574	1.704 ± 0.0036	0.2995 ± 0.0087
576	1.706 ± 0.0035	0.2996 ± 0.0085
577	1.709 ± 0.0035	0.2996 ± 0.0084
579	1.712 ± 0.0034	0.2995 ± 0.0082
580	1.714 ± 0.0034	0.2994 ± 0.0081
582	1.717 ± 0.0033	0.2993 ± 0.0079
584	1.719 ± 0.0033	0.2991 ± 0.0078
585	1.722 ± 0.0033	0.2988 ± 0.0076
587	1.725 ± 0.0033	0.2985 ± 0.0075

588	1.727 ± 0.0032	0.2981 ± 0.0073
590	1.73 ± 0.0032	0.2977 ± 0.0072
592	1.732 ± 0.0032	0.2972 ± 0.007
593	1.735 ± 0.0034	0.2967 ± 0.0069
595	1.737 ± 0.0033	0.2962 ± 0.0067
596	1.739 ± 0.0033	0.2955 ± 0.0066
598	1.742 ± 0.0033	0.2949 ± 0.0064
600	1.744 ± 0.0033	0.2942 ± 0.0063
601	1.747 ± 0.0034	0.2934 ± 0.0061
603	1.749 ± 0.0034	0.2927 ± 0.006
604	1.751 ± 0.0034	0.2918 ± 0.0059
606	1.754 ± 0.0035	0.291 ± 0.0057
608	1.756 ± 0.0035	0.2901 ± 0.0056
609	1.758 ± 0.0036	0.2891 ± 0.0055
611	1.76 ± 0.0036	0.2882 ± 0.0053
612	1.762 ± 0.0037	0.2871 ± 0.0052
614	1.765 ± 0.0038	0.2861 ± 0.0051
615	1.767 ± 0.0038	0.285 ± 0.005
617	1.769 ± 0.0039	0.2839 ± 0.0049
619	1.771 ± 0.004	0.2828 ± 0.0048
620	1.773 ± 0.0041	0.2816 ± 0.0046
622	1.775 ± 0.0042	0.2804 ± 0.0045
623	1.777 ± 0.0043	0.2792 ± 0.0044
625	1.779 ± 0.0043	0.2779 ± 0.0043
627	1.78 ± 0.0044	0.2766 ± 0.0042
628	1.782 ± 0.0047	0.2753 ± 0.004
630	1.784 ± 0.0048	0.274 ± 0.0039
631	1.786 ± 0.0049	0.2727 ± 0.0038
633	1.788 ± 0.005	0.2713 ± 0.0037
635	1.789 ± 0.0051	0.2699 ± 0.0037
636	1.791 ± 0.0052	0.2685 ± 0.0036
638	1.793 ± 0.0053	0.2671 ± 0.0035
639	1.794 ± 0.0054	0.2657 ± 0.0035
641	1.796 ± 0.0055	0.2642 ± 0.0034
643	1.797 ± 0.0056	0.2628 ± 0.0034
644	1.799 ± 0.0057	0.2613 ± 0.0033
646	1.8 ± 0.0058	0.2598 ± 0.0033
647	1.802 ± 0.0059	0.2583 ± 0.0033
649	1.803 ± 0.0061	0.2568 ± 0.0032
651	1.804 ± 0.0062	0.2553 ± 0.0032
652	1.806 ± 0.0063	0.2538 ± 0.0032

654	1.807 ± 0.0064	0.2522 ± 0.0032
655	1.808 ± 0.0065	0.2507 ± 0.0031
657	1.809 ± 0.0066	0.2492 ± 0.0031
658	1.811 ± 0.0067	0.2476 ± 0.0031
660	1.812 ± 0.0068	0.2461 ± 0.0031
662	1.813 ± 0.007	0.2445 ± 0.0031
663	1.814 ± 0.0071	0.243 ± 0.0031
665	1.815 ± 0.0072	0.2414 ± 0.0031
666	1.816 ± 0.0073	0.2398 ± 0.0031
668	1.817 ± 0.0074	0.2383 ± 0.0031
670	1.818 ± 0.0075	0.2367 ± 0.0031
671	1.819 ± 0.0076	0.2352 ± 0.0031
673	1.82 ± 0.0077	0.2336 ± 0.0032
674	1.821 ± 0.0078	0.232 ± 0.0032
676	1.822 ± 0.0079	0.2305 ± 0.0032
678	1.823 ± 0.008	0.2289 ± 0.0032
679	1.823 ± 0.0081	0.2274 ± 0.0033
681	1.824 ± 0.0082	0.2258 ± 0.0033
682	1.825 ± 0.0083	0.2243 ± 0.0033
684	1.826 ± 0.0084	0.2228 ± 0.0033
686	1.826 ± 0.0085	0.2212 ± 0.0034
687	1.827 ± 0.0086	0.2197 ± 0.0034
689	1.828 ± 0.0087	0.2182 ± 0.0035
690	1.828 ± 0.0088	0.2167 ± 0.0035
692	1.829 ± 0.0089	0.2152 ± 0.0036
694	1.829 ± 0.009	0.2137 ± 0.0036
695	1.83 ± 0.0091	0.2122 ± 0.0037
697	1.83 ± 0.0092	0.2107 ± 0.0037
698	1.831 ± 0.0093	0.2092 ± 0.0038
700	1.831 ± 0.0093	0.2078 ± 0.0038
701	1.832 ± 0.0094	0.2063 ± 0.0039
703	1.832 ± 0.0095	0.2049 ± 0.0039
705	1.833 ± 0.0096	0.2035 ± 0.004
706	1.833 ± 0.0097	0.202 ± 0.004
708	1.833 ± 0.0097	0.2006 ± 0.0041
709	1.834 ± 0.0098	0.1992 ± 0.0042
711	1.834 ± 0.0099	0.1978 ± 0.0042
713	1.834 ± 0.0099	0.1964 ± 0.0043
714	1.835 ± 0.01	0.195 ± 0.0044
716	1.835 ± 0.0101	0.1937 ± 0.0044
717	1.835 ± 0.0101	0.1923 ± 0.0045

719	1.836 ± 0.0102	0.191 ± 0.0046
721	1.836 ± 0.0103	0.1897 ± 0.0046
722	1.836 ± 0.0103	0.1883 ± 0.0047
724	1.836 ± 0.0104	0.187 ± 0.0048
725	1.836 ± 0.0104	0.1857 ± 0.0049
727	1.837 ± 0.0105	0.1844 ± 0.0049
729	1.837 ± 0.0105	0.1832 ± 0.005
730	1.837 ± 0.0106	0.1819 ± 0.0051
732	1.837 ± 0.0106	0.1807 ± 0.0052
733	1.837 ± 0.0107	0.1794 ± 0.0052
735	1.837 ± 0.0107	0.1782 ± 0.0053
736	1.837 ± 0.0108	0.177 ± 0.0054
738	1.837 ± 0.0108	0.1758 ± 0.0055
740	1.837 ± 0.0108	0.1746 ± 0.0055
741	1.838 ± 0.0109	0.1734 ± 0.0056
743	1.838 ± 0.0109	0.1722 ± 0.0057
744	1.838 ± 0.0109	0.1711 ± 0.0058
746	1.838 ± 0.011	0.1699 ± 0.0059
748	1.838 ± 0.011	0.1688 ± 0.0059
749	1.838 ± 0.011	0.1677 ± 0.006
751	1.838 ± 0.0111	0.1666 ± 0.0061
752	1.838 ± 0.0111	0.1655 ± 0.0062
754	1.838 ± 0.0111	0.1644 ± 0.0063
756	1.838 ± 0.011	0.1633 ± 0.0063
757	1.838 ± 0.0111	0.1622 ± 0.0064
759	1.838 ± 0.0112	0.1612 ± 0.0065
760	1.838 ± 0.0112	0.1601 ± 0.0066
762	1.837 ± 0.0112	0.1591 ± 0.0067
763	1.837 ± 0.0112	0.1581 ± 0.0067
765	1.837 ± 0.0112	0.1571 ± 0.0068
767	1.837 ± 0.0112	0.1561 ± 0.0069
768	1.837 ± 0.0112	0.1551 ± 0.007
770	1.837 ± 0.0112	0.1541 ± 0.0071
771	1.837 ± 0.0112	0.1532 ± 0.0071
773	1.837 ± 0.0113	0.1522 ± 0.0072
775	1.837 ± 0.0113	0.1513 ± 0.0073
776	1.837 ± 0.0113	0.1503 ± 0.0074
778	1.837 ± 0.0113	0.1494 ± 0.0075
779	1.836 ± 0.0113	0.1485 ± 0.0075
781	1.836 ± 0.0113	0.1476 ± 0.0076
783	1.836 ± 0.0113	0.1467 ± 0.0077

784	1.836 ± 0.0113	0.1458 ± 0.0078
786	1.836 ± 0.0112	0.1449 ± 0.0079
787	1.836 ± 0.0112	0.1441 ± 0.0079
789	1.836 ± 0.0112	0.1432 ± 0.008
790	1.836 ± 0.0113	0.1424 ± 0.008
792	1.835 ± 0.0113	0.1416 ± 0.008
794	1.835 ± 0.0113	0.1407 ± 0.0081
795	1.835 ± 0.0113	0.1399 ± 0.0082
797	1.835 ± 0.0113	0.1391 ± 0.0083
798	1.835 ± 0.0113	0.1383 ± 0.0083
800	1.835 ± 0.0112	0.1375 ± 0.0084

Use of an impactor to reduce multiply charged particles

PAS signal due to light absorption by size selected dry nigrosin particles was measured and compared to absorption coefficient (α_{abs}) calculated using a Mie theory routine. To reduce errors in the calculation of α_{abs} the concentration and size of the measured particles needs to be accurately characterized.

In order to reduce uncertainty in size distribution of the size selected quasi-monodispersed aerosols the fraction of multiply charged particles (MCP) needs to be quantified (Wiedensohler, 1988; Hasenkopf et al., 2010; Bluvshtein et al., 2012; Washenfelder et al., 2013) or significantly reduced.

To reduce the fraction of MCP in aerosolized, size selected aerosols, the solution concentration was reduced (0.1 to 0.5 gr L^{-1}, depending on required particle size) and the atomizer inlet pressure was increased (35 PSIG). More importantly an impactor was used on the DMA inlet. The impactors' 50% collection efficiency (or cut-off diameter, d_{50}) is described by (Hinds, 1999):

$$d_{50} = -0.078 + \sqrt{\left[\frac{9\pi\eta D_j^3 (Stk_{50})}{4\rho_p Q}\right]} \quad [\mu m] \qquad (S1)$$

where η is the gas viscosity (1.756×10^{-5} kg m^{-1} sec^{-1} for nitrogen at 22 ^{0}C), D_j is the nozzle diameter (457 μm), Stk_{50} is the Stokes number (0.24 unitless, for circular jet), ρ_p is the particle density (1.6 gr cm^{-3}, density of nigrosin (Moteki et al., 2010)) and Q is the volumetric flow rate of the sample flow.

As explained in the main text, nigrosin particles with diameters of 250 to 325 nm (at 25 nm steps) were size selected and the sample flow (and sheath flow) into the DMA was adjusted (520 to 750 cm^3 min^{-1}) so that d_{50} was 50 nm larger than the selected diameter.

Additional references

Bluvshtein, N., Flores, J. M., Riziq, A. A., and Rudich, Y.: An approach for faster retrieval of aerosols' complex refractive index using cavity ring-down spectroscopy, 46, 10.1080/02786826.2012.700141, 2012.

Hasenkopf, C. A., Beaver, M. R., Trainer, M. G., Dewitt, H. L., Freedman, M. A., Toon, O. B., McKay, C. P., and Tolbert, M. A.: Optical properties of titan and early earth haze laboratory analogs in the mid-visible, Icarus, 207, 10.1016/j.icarus.2009.12.015, 2010.

Hinds, W. C.: Aerosol technology : Properties, behavior, and measurement of airborne particles, in, Wiley, New York, 121-128, 1999.

Moteki, N., Kondo, Y., Nakayama, T., Kita, K., Sahu, L. K., Ishigai, T., Kinase, T., and Matsumi, Y.: Radiative transfer modeling of filter-based measurements of light absorption by particles: Importance of particle size dependent penetration depth, J. Aerosol. Sci., 41, 10.1016/j.jaerosci.2010.02.002, 2010.

Washenfelder, R. A., Flores, J. M., Brock, C. A., Brown, S. S., and Rudich, Y.: Broadband measurements of aerosol extinction in the ultraviolet spectral region, Atmos Meas Tech, 6, 10.5194/amt-6-861-2013, 2013.

Wiedensohler, A.: An approximation of the bipolar charge distribution for particles in the submicron size range, 19, http://dx.doi.org/10.1016/0021-8502(88)90278-9, 1988.